



Site occupancy and luminescence of Ce³⁺ ions in whitlockite-related strontium lutetium phosphate

Yongqiang Geng^{a,b}, Qiufeng Shi^{a,*}, Fangtian You^c, Konstantin V. Ivanovskikh^d, Ivan I. Leonidov^{e,f}, Ping Huang^a, Lei Wang^a, Yue Tian^a, Yan Huang^g, Cai'e Cui^{a,*}

^a College of Physics and Optoelectronics, Taiyuan University of Technology, Taiyuan 030024, China

^b Key Lab of Advanced Transducers and Intelligent Control System of Ministry of Education, Taiyuan University of Technology, Taiyuan 030024, China

^c Key Laboratory of Luminescence and Optical Information, Ministry of Education, Institute of Optoelectronic Technology, Beijing Jiaotong University, Beijing 100044, China

^d Institute of Physics and Technology, Ural Federal University, 620002, Ekaterinburg, Russia

^e School of Engineering, Ural Federal University, 620002, Ekaterinburg, Russia

^f Institute of High-Temperature Electrochemistry, UB RAS, 620137, Ekaterinburg, Russia

^g Beijing Synchrotron Radiation Facilities, Institute of High Energy Physics, Chinese Academy of Sciences, Beijing 100039, China

ARTICLE INFO

Keywords:

Whitlockites
Ce³⁺ 5d-4f emission
Crystallographic sites
UV-VUV spectroscopy
Decay curves

ABSTRACT

Ce³⁺-doped Sr₉Lu(PO₄)₇ polycrystalline material has been synthesized using a solid state reaction at high temperature. Luminescence spectroscopic properties and emission decay kinetics have been studied upon UV-VUV excitation. Emission from Ce³⁺ ions located in two types of crystallographic sites has been identified in low-temperature spectra. Ce³⁺ ions have been shown to prefer occupying Sr²⁺ sites rather than Lu³⁺ sites. The temperature-dependent decay curves of Ce³⁺ 5d→4f emission demonstrate an excellent luminescence thermal stability.

1. Introduction

Cerium-doped luminescent inorganic materials have deserved great attention of the researchers over the last two decades while considered to be promising for application as phosphors for white light-emitting diodes (WLEDs), fluorescent tubes and CRT and as phosphors and scintillators for detectors of ionizing radiation [1–10]. Due to the strong influence of local environment to 5d electron, luminescence properties of crystals doped with Ce³⁺ ions are host dependent. In other words, the 5d energy level structure, crystal field splitting, Stokes shift, location of 5d levels relative to the host bands and some other properties vary significantly in different materials, that have been systematically studied by Dorenbos while analyzing a large number of the reported data [11–15].

Our search for new promising materials for scintillation application has led us to the synthesis and study of the double phosphate Sr₉Lu(PO₄)₇ doped with Ce³⁺ ions. The whitlockite-type phosphates M₉²⁺R(PO₄)₇ (M = Ca, Mg, Zn, Sr; R = Cr, Ga, In or rare-earth ions) and their derivatives have been widely studied in different fields of materials over the last two decades. Many β-Ca₃(PO₄)₂-related compounds [16] including Ca₉R(AO₄)₇ and Ca₈MgR(AO₄)₇ (A = P and V; R = Cr, Ga, In

or rare-earth ions) are found to be materials for solid state lighting [17–22] and bioimaging [23] applications, laser systems [24] and non-linear optical devices [25,26]. Many of these complex oxides are known as ferroelectrics [25,27], antiferroelectrics [28,29] and catalysts [30]. On the one hand, substitution of Ca²⁺ with divalent ions with smaller ionic radii (e.g., with Mg²⁺) in the crystal structure of Ca₉R(PO₄)₇ promotes the formation of Ca₈M²⁺R(PO₄)₇ and slows degradation of polar structures to centrosymmetric ones that implies the changing of the space group from R3c to R3c or R3m [29,31]. On the other hand, the presence of dopant cations with large radii (e.g., Pb²⁺) in the lattice of Ca₈M²⁺R(PO₄)₇ does not lead to nonpolar structure and the space group R3c, in which the compound crystallizes, remains [32]. When Ca is substituted by Sr, the crystal structure changes to monoclinic one that is described in the space group I2/a [33]. Optical spectroscopy studies of Sr₉Sc(PO₄)₇ [34] and Sr₉Lu(PO₄)₇:Eu²⁺, Mn²⁺ [35], Sr₉Sc(PO₄)₇:Ce³⁺, Mn²⁺ [36], Sr₉In_{1-x}Lu_x(PO₄)₇:Eu²⁺ [37] and Sr₉A(PO₄)₇ (A = In, Ga):Eu³⁺ [38] have confirmed the significant potential of the corresponding whitlockite-related hosts for the development of new series of WLED phosphors.

The Sr₉Lu(PO₄)₇ host lattice possesses many advantages, such as good chemical stability, easy chemical routes for the preparation,

* Corresponding author.

E-mail addresses: shiqiufeng@tyut.edu.cn (Q. Shi), tytgcejy@sina.com (C. Cui).

<https://doi.org/10.1016/j.matresbull.2019.04.014>

Received 18 March 2019; Received in revised form 5 April 2019; Accepted 9 April 2019

Available online 10 April 2019

0025-5408/ © 2019 Elsevier Ltd. All rights reserved.

relatively large bandgap energy and large effective atomic number of 38.9, that makes it challenging to test it as a host for Ce^{3+} doping and potential scintillator applications. However, luminescence spectroscopic properties of Ce^{3+} -activated $\text{Sr}_9\text{Lu}(\text{PO}_4)_7$ have not been studied yet. Note that Ce^{3+} ion demonstrates site-dependent luminescence properties while having the most simple electronic structure among the lanthanide series and is widely used as an optical probe to understand the crystal field strength and local structure features [4,12–15,39,40].

The present paper is focused on low temperature luminescence VUV-UV spectroscopy as well as luminescence decay measurements of Ce^{3+} -doped $\text{Sr}_9\text{Lu}(\text{PO}_4)_7$. Furthermore, Ce^{3+} 5d energy level structure and site occupation preferences are studied and identified.

2. Experimental

2.1. Sample preparation

The powder sample of $\text{Sr}_9\text{Lu}(\text{PO}_4)_7:0.5\%\text{Ce}^{3+}$ was prepared by a conventional solid-state reaction. The stoichiometrically weighed reactants of SrCO_3 (A.R.), $\text{NH}_4\text{H}_2\text{PO}_4$ (A.R.), CeO_2 (99.9%), Lu_2O_3 (99.99%) with 5 wt% of H_3BO_3 (A.R.), added as fluxing agent, were first thoroughly ground in an agate mortar and pre-sintered in alumina crucible at 873 K for 3 h, and then sintered at 1563 K for 3 h in a CO-reducing atmosphere. Finally, the as-synthesized material was left in the off-switched furnace to get slowly (naturally) cooled down to the room temperature in a continuous CO flow. The resulting material was ground again into a white powder.

2.2. Characterization

Powder X-ray diffraction (XRD) patterns were collected using a Shimadzu XRD-6000 X-ray diffractometer operating at 40 kV and 30 mA with $\text{Cu K}\alpha$ ($\lambda = 1.5406 \text{ \AA}$) radiation in the 2θ range from 10° to 60° with a step of 0.01° . XRD analysis was carried out employing the ICSD-Web database (2018/II).

The measurements of excitation and emission spectra upon excitation with VUV-UV synchrotron radiation were performed using a VUV spectroscopy setup mounted at the Beamline 4B8 of Beijing Synchrotron Radiation Facilities (BSRF). Technical characteristics of the setup were briefly described in Ref. [41]. The samples were mounted on a closed-cycle helium cryostat holder (Janis CCS-UHV/204) that allows temperature varying from 10 to 300 K. All the excitation spectra were corrected with the real time excitation spectrum of sodium salicylate for the wavelength-dependent variation of the incident light intensity and excitation monochromator response.

The decay curves were recorded using an Edinburgh Instruments FLS980 fluorescence spectrometer equipped with a cooled single-photon counting photomultiplier tube (Hamamatsu R928 P) as detector and a 30 W nanosecond flash lamp (pulse width ~ 1 ns, pulse rate 40–100 kHz) filled with hydrogen as an excitation source (wavelength 200–400 nm). The sample was mounted on a sample holder of an Oxford Instruments Microstat N2 cryostat cooled with liquid nitrogen. The temperature was adjusted from 78 to 300 K. For the measurement in the temperature range from 300 to 650 K, a home-made setup of temperature control system was used, with temperature accuracy of about ± 0.5 K.

3. Results and discussion

3.1. Crystal structure

The whitlockite-related phosphates $\text{Sr}_9\text{A}(\text{PO}_4)_7$ ($\text{A} = \text{Sc}, \text{Cr}, \text{Fe}, \text{Ga}, \text{In}$) and $\text{Sr}_9\text{R}(\text{PO}_4)_7$ ($\text{R} = \text{Tm-Lu}$) have been earlier shown to be isostructural and adopt the symmetry of the space group $\text{C}2/m$, $Z = 4$, for their unit cells [42]. However, a detailed crystal structure refinement supported by selected area electron diffraction has revealed the

conclusive evidence that $\text{Sr}_9\text{A}(\text{PO}_4)_7$ ($\text{A} = \text{Sc}, \text{Cr}, \text{Fe}, \text{Ga}, \text{In}$) are nevertheless centrosymmetric while the lattice is characterized by the symmetry of space group $I2/a$, $Z = 4$ [42,43]. Crystal radii of A^{3+} ($\text{A} = \text{Sc}, \text{Cr}, \text{Fe}, \text{Ga}, \text{In}$) and R^{3+} ($\text{R} = \text{Tm-Lu}$) sites in 6-fold coordination vary from 0.755 \AA ($r^{\text{VI}}(\text{Cr}^{3+})$) to 0.930 \AA ($r^{\text{VI}}(\text{In}^{3+})$) and from 1.001 \AA ($r^{\text{VI}}(\text{Lu}^{3+})$) to 1.020 \AA ($r^{\text{VI}}(\text{Tm}^{3+})$), respectively [44,45]. Note that the relative difference between the smallest $r^{\text{VI}}(\text{Cr}^{3+})$ and the largest $r^{\text{VI}}(\text{Tm}^{3+})$ is 35.1%. Therefore, the compounds $\text{Sr}_9\text{A}(\text{PO}_4)_7$ ($\text{A} = \text{Sc}, \text{Cr}, \text{Fe}, \text{Ga}, \text{In}, \text{Tm-Lu}$) are featured by a high unit cell capacity as all of them crystallize in the space group $I2/a$, $Z = 4$ [42,43].

Although gadolinium and terbium $\beta\text{-Ca}_3(\text{PO}_4)_2$ -related phosphates can be easily prepared via the solid-state reaction [46], the phases $\text{Sr}_9\text{R}(\text{PO}_4)_7$ ($\text{R} = \text{Gd}, \text{Tb}$) usually contain trace impurities of eulytite-type $\text{Sr}_3\text{R}(\text{PO}_4)_3$ ($\text{R} = \text{Gd}$ ($\sim 7\%$) and Tb ($\sim 2\%$)). Obviously, at one annealing temperature, the quantity of an impurity in $\text{Sr}_9\text{R}(\text{PO}_4)_7$ ($\text{R} = \text{Y}$ and Gd-Lu) grows when crystal radius of lanthanide cations increases. For one composition, the quantity of the impurity increases simultaneously with annealing temperature. The real composition of a phase related to $\beta\text{-Ca}_3(\text{PO}_4)_2$ is also written as $\text{Sr}_{9+1.5x}\text{R}_{1-x}(\text{PO}_4)_7$, $\text{R} = \text{Y}$ and Gd-Lu [46]. Whitlockite-related compounds are not found in the group of $\text{Sr}_9\text{R}(\text{PO}_4)_7$, $\text{R} = \text{La-Sm}$ [43,46], whereas the sample with the nominal composition of $\text{Sr}_9\text{Eu}(\text{PO}_4)_7$ contains just a large amount of $\text{Sr}_3(\text{PO}_4)_2$ and $\text{Sr}_3\text{Eu}(\text{PO}_4)_3$ in addition to the $\beta\text{-Ca}_3(\text{PO}_4)_2$ -related phase [46]. Employing Eu^{3+} ion as optical probe, Ma et al. have recently proved that both Sr^{2+} and R^{3+} ($\text{R} = \text{In}, \text{Ga}$) ions in their corresponding noncentrosymmetric (Sr^{2+}) and centrosymmetric (R^{3+}) sites can be substituted by lanthanides in $\text{Sr}_9\text{R}(\text{PO}_4)_7$, $\text{R} = \text{In}, \text{Ga}$ [38]. Given the observations listed above, we conclude about the possibility of doping $\text{Sr}_9\text{Lu}(\text{PO}_4)_7$ with relatively low concentration of Ce^{3+} that in turn is revealed with the powder XRD study of $\text{Sr}_9\text{Lu}(\text{PO}_4)_7:0.5\%\text{Ce}^{3+}$ (Fig. 1).

As long as there are no cards for $\text{Sr}_9\text{Lu}(\text{PO}_4)_7$ and $\text{Sr}_3\text{Lu}(\text{PO}_4)_3$ available in the ICSD-Web database (2018/II), the XRD patterns of the counterparts $\text{Sr}_9\text{In}(\text{PO}_4)_7$ (ICSD #59,722; [42]) and $\text{Sr}_3\text{Lu}(\text{PO}_4)_3$ (PDF #33-1344) have been taken into consideration. The powder XRD pattern of $\text{Sr}_9\text{Lu}(\text{PO}_4)_7:0.5\%\text{Ce}^{3+}$ is found to agree well with the main phase of $\text{Sr}_9\text{Lu}(\text{PO}_4)_7$ while indicating the presence of ca. 6–7% $\text{Sr}_3\text{Lu}(\text{PO}_4)_3$ which is isotypic to $\text{Sr}_3\text{Y}(\text{PO}_4)_3$ [47] in the prepared sample (Fig. 1). This result stays in line with the crystallographic studies of isostructural $\text{Sr}_9\text{R}(\text{PO}_4)_7$ ($\text{R} = \text{In}, \text{Gd}$) where crystal radii of R^{3+} ions in 6-fold coordination are $r^{\text{VI}}(\text{In}^{3+}) = 0.93 \text{ \AA}$ and $r^{\text{VI}}(\text{Gd}^{3+}) = 1.078 \text{ \AA}$ [44,45]. The relative difference between these values counts 15.9%. In contrast to $\text{Sr}_9\text{In}(\text{PO}_4)_7$ which exists as a single phase, the formation of $\text{Sr}_9\text{Gd}(\text{PO}_4)_7$ is followed by the presence of ~ 7 wt% $\text{Sr}_3\text{Gd}(\text{PO}_4)_3$ [46]. Crystal radii of Ce^{3+} and Lu^{3+} in 6-fold coordination in the lattice of $\text{Sr}_9\text{R}(\text{PO}_4)_7$ ($\text{R} = \text{Ce}, \text{Ln}$) are $r^{\text{VI}}(\text{Ce}^{3+}) = 1.150 \text{ \AA}$ and $r^{\text{VI}}(\text{Lu}^{3+}) = 1.001 \text{ \AA}$, respectively, that gives the relative difference of 14.9%.

In summary, $\text{Sr}_9\text{Lu}(\text{PO}_4)_7:0.5\%\text{Ce}^{3+}$ crystallizes in the monoclinic

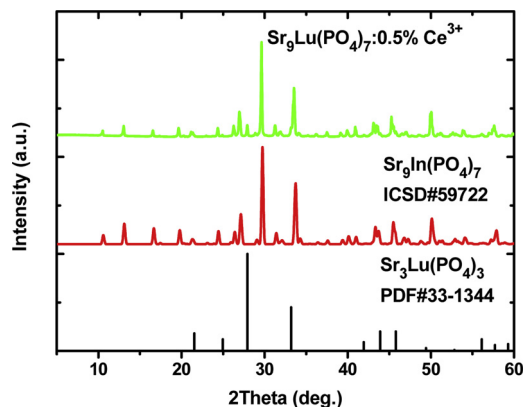


Fig. 1. Powder XRD pattern of $\text{Sr}_9\text{Lu}(\text{PO}_4)_7:0.5\%\text{Ce}^{3+}$ and standard cards of $\text{Sr}_9\text{In}(\text{PO}_4)_7$ and $\text{Sr}_3\text{Lu}(\text{PO}_4)_3$.

space group $I2/a$, $Z = 4$ [46]. The asymmetric unit is characterized by five crystallographically nonequivalent sites (8f) of Sr with the C_1 symmetry, one position (4a) of Lu with the C_i symmetry, four P, and fourteen O sites. The Sr (2) and Sr (1, 3, 4, 5) sites are coordinated by eight and nine oxygen atoms, respectively. Therefore, one can conclude that there are two types of strontium sites in the unit cell of the $\text{Sr}_9\text{Lu}(\text{PO}_4)_7$ host. The crystal radii of Sr^{2+} cations located in the positions with coordination numbers $\text{CN} = 8$ and $\text{CN} = 9$ are $r^{\text{VIII}}(\text{Sr}^{2+}) = 1.390 \text{ \AA}$ and $r^{\text{IX}}(\text{Sr}^{2+}) = 1.425 \text{ \AA}$, respectively [44,45]. In turn, Sr^{2+} can be substituted with Ce^{3+} in the sites of both types as the corresponding values of $r^{\text{VIII}}(\text{Ce}^{3+})$ and $r^{\text{IX}}(\text{Ce}^{3+})$ are 1.270 \AA and 1.320 \AA , respectively. Therefore, similar to Eu^{3+} -doped $\text{Sr}_9\text{In}(\text{PO}_4)_7$ [38], $\text{Sr}_9\text{Lu}(\text{PO}_4)_7$ doped with Ce^{3+} is featured by the presence of Ce^{3+} in crystallographic sites of C_1 (8- and 9-fold coordination) and C_i symmetry (6-fold coordination). Considering the structural chemistry of $\text{Sr}_9\text{Lu}(\text{PO}_4)_7:\text{Ce}^{3+}$ discussed above, Ce^{3+} ions are expected to occupy both lutetium (C_i) and more predominantly strontium (C_1) sites as there are 144 strontium (C_1) ones and just 16 lutetium (C_i) positions per unit cell. This along with concentration quenching, previously analyzed for isostructural lanthanide-doped $\text{Sr}_9\text{In}(\text{PO}_4)_7$ [38], may lead to the fact that emission from Ce^{3+} ions located in the Lu^{3+} sites is either insignificant, or hardly distinguished in luminescence spectra of $\text{Sr}_9\text{Lu}(\text{PO}_4)_7:0.5\%\text{Ce}^{3+}$.

3.2. Luminescence VUV spectroscopy and Ce^{3+} site occupancy

In order to probe the dopant sites of Ce^{3+} in $\text{Sr}_9\text{Lu}(\text{PO}_4)_7:\text{Ce}^{3+}$, low temperature emission and excitation spectra of $\text{Sr}_9\text{Lu}(\text{PO}_4)_7:0.5\%\text{Ce}^{3+}$ have been studied. Fig. 2 demonstrates emission spectra recorded upon excitation at 3.76 eV (330 nm) and 4.77 eV (260 nm) at $T = 10 \text{ K}$. The former consists of a typical $\text{Ce}^{3+} 5d \rightarrow 4f$ doublet emission band that can be fitted with two Gaussians, centered near 3.09 eV (401 nm) and 3.34 eV (371 nm) (Fig. 2a). We note that the fitting the $5d \rightarrow 4f$ emission with Gaussians is quite relative and is rather used for simplicity, while normally the $5d \rightarrow 4f$ emission (as well as $4f \rightarrow 5d$ excitation) bands have a Pekar-like shape that is typical for electronic transitions characterized by Huang-Rhys parameter close to 1 [48,49]. The energy difference between the two Gaussian bands is $\sim 0.25 \text{ eV}$, that is very typical value for the energy difference between ${}^2F_{7/2}$ and ${}^2F_{5/2}$ states of Ce^{3+} . Accordingly, these two emission Gaussian bands are attributed to Ce^{3+} radiative transitions from $5d$ to ${}^2F_{7/2}$ and ${}^2F_{5/2}$ states, respectively. Upon excitation at 4.77 eV (260 nm), a much broader emission band is revealed (Fig. 2(b)). In addition to the two emission bands as fitted in Fig. 2(a), other two bands can be distinguished at the high

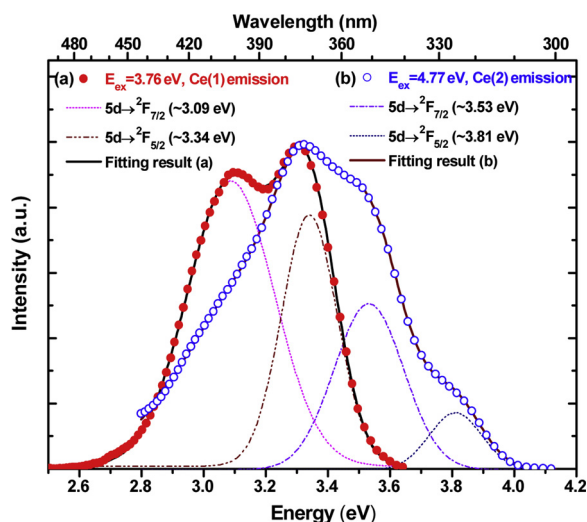


Fig. 2. Emission spectra of $\text{Sr}_9\text{Lu}(\text{PO}_4)_7:0.5\%\text{Ce}^{3+}$ upon excitation at $E_{\text{ex}} = 3.76 \text{ eV}$ (a) and $E_{\text{ex}} = 4.77 \text{ eV}$ (b) at $T = 10 \text{ K}$.

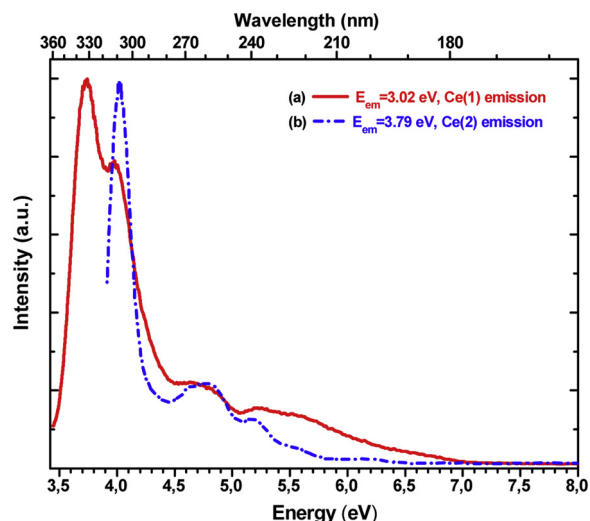


Fig. 3. Excitation spectra of $\text{Sr}_9\text{Lu}(\text{PO}_4)_7:0.5\%\text{Ce}^{3+}$ recorded monitoring Ce(1) emission at $E_{\text{em}} = 3.02 \text{ eV}$ (a) and Ce(2) emission $E_{\text{em}} = 3.79 \text{ eV}$ (b) at $T = 10 \text{ K}$.

energy side by applying the Gaussian fitting. The latter suggests the presence of two peaks, centered near 3.53 eV (351 nm) and 3.81 eV (325 nm), which remain a typical Ce^{3+} doublet emission band. (The two low energy Gaussians in the fitting of the 4.77 eV excited spectrum are not shown for brevity). Finally, two types of $\text{Ce}^{3+} 5d \rightarrow 4f$ luminescence located in the violet and UV regions are disclosed and are further denoted as Ce(1) and Ce(2) emissions. Note that upon excitation at 3.76 eV, only Ce(1) emission is observed while excitation at 4.77 eV gives rise to the observation of both the emission features that makes the corresponding emission spectrum more complex and broad (Fig. 2).

The presence of the $\text{Ce}^{3+} 5d \rightarrow 4f$ emission from two different types of crystallographic sites is further demonstrated with excitation spectra measurements performed at $T = 10 \text{ K}$ (Fig. 3). The spectrum recorded monitoring Ce(1) emission at 3.02 eV (411 nm) reveals the onset related to the beginning of Ce(1) $4f \rightarrow 5d$ excitation transitions at about 3.45 eV (359 nm) that is followed by the strong doublet excitation feature with peaks located near 3.73 eV (332 nm) and 3.97 eV (312 nm). Other Ce(1) excitation features are less pronounced and appear as enhancements centered 4.72 eV (263 nm), 5.21 eV (238 nm), and broader complex feature spread up to about 7 eV. In turn, the spectrum recorded monitoring Ce(2) emission at 3.79 eV (327 nm) reveals the beginning of $4f \rightarrow 5d$ transitions at about 3.90 eV (318 nm) with the first excitation peak at 4.02 eV (308 nm). Less intense but still well pronounced broad excitation features are observed to center near 4.76 eV (261 nm) and 5.19 eV (239 nm). Weak enhancements in the Ce(2) excitation spectrum are also observed at 5.60 eV (221 nm) and 6.40 eV (194 nm). The observed features in Ce(1) and Ce(2) excitation spectra are assigned to the transitions from the ${}^2F_{5/2}$ ground state to the different levels of the $5d$ configuration of Ce^{3+} . Note that some excitation bands appear in both the spectra that may indicate the presence of an energy transfer between the emission centers of two types. The energy transfer can be realized through reabsorption of Ce(2) emission by the emission centers responsible for Ce(1) emission. This is favorable due to the overlap of Ce(2) emission and the most intense Ce(1) excitation band in the range of about 3.5–4.0 eV (Figs. 2 and 3). It is worth mentioning that the reabsorption can be responsible for unusual relative intensities of Ce(2) doublet components where high-energy part (related to relaxation into the ${}^2F_{5/2}$ ground state) is noticeably suppressed. Table 1 gathers information about the observed Ce^{3+} emission features.

To further identify the site occupancy, a crystal-field splitting (CFS) should be considered which is related to the shape and size of the anion coordination polyhedron [15]. Generally, with the increase of

Table 1

Absorption (E_{ex}) and emission (E_{em}) energies, and Stokes shift ($\Delta S(\text{\AA})$) for two types of Ce^{3+} emission observed in $\text{Sr}_9\text{Lu}(\text{PO}_4)_7$ spectra.

Emission type	E_{ex} (eV)	E_{em} (eV)	ΔS (eV)
1	3.73	3.32	0.41
2	4.02	3.81	0.21

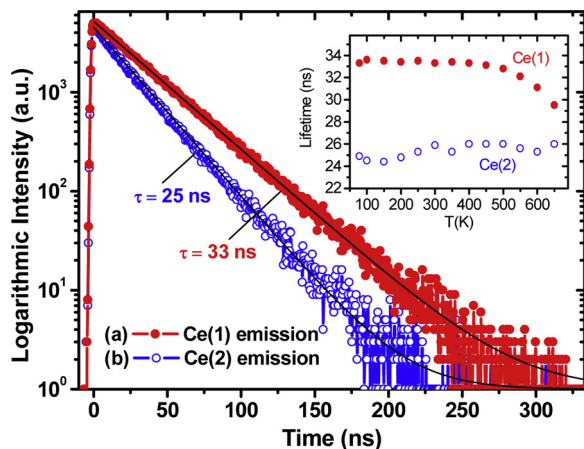


Fig. 4. Luminescence decay curves recorded at $T = 78$ K monitoring Ce(1) at $E_{em} = 3.87$ eV and Ce(2) emission at $E_{em} = 3.10$ eV upon excitation at $E_{ex} = 4.77$ eV, and $E_{ex} = 3.75$ eV, respectively. Inset shows temperature dependence of Ce(1) and Ce(2) emission lifetime.

coordination number and bond length, the CFS decreases. The average bond length of nine coordinated Sr(1), Sr(3), Sr(4) and Sr(5) sites is nearly the same being about 2.70 Å. The average bond length for eight coordinated Sr(2) site is about 2.6 Å. According to the inverse relationship of the CFS to the bond length and the coordination number, the Ce^{3+} ions responsible for the lower energy Ce(1) emission should substitute for Sr(2) sites. The Ce^{3+} ions with smaller CFS located in Sr(1), Sr(3), Sr(4) and Sr(5) sites are responsible for the higher energy Ce(2) emission. Because of very similar bond length and the same coordination number of the Sr(1), Sr(3), Sr(4) and Sr(5) sites, the corresponding emissions appear the same way in the spectra.

Manifestation of Ce^{3+} ions appeared in the $\text{Sr}_3\text{Lu}(\text{PO}_4)_3$ phase cannot be reasonably distinguished in the presented emission and excitation spectra. On the one hand, this is explained by obviously low content of the $\text{Sr}_3\text{Lu}(\text{PO}_4)_3$ phase. On the other hand, the coordination number of Sr^{2+} and mean values of Sr–O bond lengths in the cells of $\text{Sr}_9\text{R}(\text{PO}_4)_7$ and $\text{Sr}_3\text{R}(\text{PO}_4)_3$ ($R = \text{Y, In, Lu}$) are almost identical [42,46,47]. This suggests that crystal field parameters for Ce^{3+} ions located in Sr(1), Sr(3), Sr(4) and Sr(5) sites in $\text{Sr}_9\text{Lu}(\text{PO}_4)_7$ are very similar to those for Ce^{3+} in the $\text{Sr}_3\text{Lu}(\text{PO}_4)_3$ phase with small amount in $\text{Sr}_9\text{Lu}(\text{PO}_4)_7$. Therefore, emission bands from Ce^{3+} in the $\text{Sr}_3\text{Lu}(\text{PO}_4)_3$ phase are expected to overlap with those related to Ce(2) emission in $\text{Sr}_9\text{Lu}(\text{PO}_4)_7$. The latter is another reason that contribution to emission spectra from Ce^{3+} ions located in the lattice of $\text{Sr}_3\text{Lu}(\text{PO}_4)_3$ can be neglected.

Host-related contribution to the excitation spectra are not expected to be induced as a typical bandgap of double phosphates is related to much wider ranges from about 8–9.3 eV [50–52] that exceeds the upper energy limit of the VUV setup used for the performed measurements.

3.3. Temperature-dependent decay time measurements

As discussed in the previous section of the emission and excitation spectra (Figs. 2 and 3), there are two types of Ce^{3+} emission related to the different (groups of) crystallographic sites of Ce^{3+} in $\text{Sr}_9\text{Lu}(\text{PO}_4)_7$. Accordingly, luminescence decay curves for the two Ce^{3+} emission

types monitored at 320 nm and 400 nm at 78 K are presented in Fig. 4. Both the decay curves are satisfactory fitted with a single exponential decay function. The fitting results suggest that at $T = 78$ K the lifetime of Ce(1) and Ce(2) emission features is 33 and 25 ns, respectively. Note, that the lifetime of Ce^{3+} ions responsible for higher energy Ce(2) emission is shorter than that observed for lower energy Ce(1) emission being in agreement with Fermi's Golden Rule. The measured $\text{Ce}^{3+} 4f \rightarrow 5d$ emission lifetime is consistent with that for some other Ce^{3+} -doped double phosphates, e.g., $\text{Li}_3\text{Lu}(\text{PO}_4)_2$ ($\tau \approx 20$ ns) [5], $\text{K}_3\text{Lu}(\text{PO}_4)_2$ (two emission sites with $\tau_1 \approx 25$ ns $\tau_2 \approx 34$ ns) [6], $\text{Ca}_9\text{Lu}(\text{PO}_4)_7$ (29 ns) [22].

The inset in Fig. 4 represents temperature dependences of Ce(1) and Ce(2) emission lifetimes. Both the emissions demonstrate a quite good thermal stability over the wide temperature range. While Ce(1) emission reveals firm tendency to decay above 500 K it is quite hard to apply any quenching model to the observed dependence due to the low variation of the measured lifetime through the entire temperature range.

Given that the decay curves recorded for Ce(1) and Ce(2) emissions keep single exponential decay behavior, one can conclude that the presence of other types of Ce^{3+} emission centers is negligible. Among those, there are Ce^{3+} ions substituting for Lu^{3+} sites and trace amounts of Ce^{3+} which may be adopted the $\text{Sr}_3\text{Lu}(\text{PO}_4)_3:\text{Ce}^{3+}$ phase.

4. Conclusions

Ce^{3+} -doped $\text{Sr}_9\text{Lu}(\text{PO}_4)_7$ can be prepared through high-temperature solid-state reaction method. Whitlockite-related $\text{Sr}_9\text{Lu}(\text{PO}_4)_7:0.5\%\text{Ce}^{3+}$ crystallizes with monoclinic unit cells $I2/a$, $Z = 4$. Two types of $\text{Ce}^{3+} 5d \rightarrow 4f$ emission centers have been observed and determined through low-temperature UV-VUV spectroscopic study. It has been shown that Ce^{3+} ions responsible for lower energy Ce(1) emission substitute for Sr(2) sites while those located in Sr(1), Sr(3), Sr(4) and Sr(5) sites are responsible for higher energy Ce(2) emission. The $\text{Ce}^{3+} 5d \rightarrow 4f$ emission of both types demonstrates good thermal stability that makes $\text{Sr}_9\text{Lu}(\text{PO}_4)_7:\text{Ce}^{3+}$ to be promising material for solid state lighting or scintillation applications.

Acknowledgments

We are grateful to Dr. Alexei A. Belik (National Institute for Materials Science, Tsukuba, Japan) for fruitful discussions. The work was financially supported by the Natural Science Foundation of Shanxi Province (201701D221009, 201801D121020, and 201801D221132), school fund of Taiyuan University of Technology (1205-04020102, 2015QN068, tyut-rc201497a). K.V.I. and I.L.L. acknowledge partial support from the UrFU Competitiveness Enhancement Program.

References

- [1] Z. Xia, A. Meijerink, *Chem. Soc. Rev.* 46 (2017) 275–299.
- [2] M. Nikl, A. Yoshikawa, *Adv. Opt. Mater.* 3 (2015) 463–481.
- [3] M. Conti, L. Eriksson, H. Rothfuss, C.L. Melcher, *IEEE Trans. Nucl. Sci.* 56 (2009) 926–933.
- [4] Y. Zorenko, V. Gorbenko, J. Vasylykiv, A. Zelenyj, A. Fedorov, R. Kucerkova, J.A. Mares, M. Nikl, P. Bilski, A. Twardak, *Mater. Res. Bull.* 64 (2015) 355–363.
- [5] D. Wisniewski, L.A. Boatner, *IEEE Trans. Nucl. Sci.* 56 (2009) 3806–3818.
- [6] D. Wisniewski, A.J. Wojtowicz, W. Drozdowski, J.M. Farmer, L.A. Boatner, *Cryst. Res. Technol.* 38 (2003) 275–282.
- [7] L.J. Dai, S.X. Huang, Y. Zhong, Z.W. Rang, Z. Zhou, *Mater. Res. Bull.* 93 (2017) 251–255.
- [8] W.R. Wang, Y.Q. Yang, Y.L. Liu, D. Pan, X. Luo, S. Yan, G.T. Xiang, Y. Jin, *Mater. Res. Bull.* 101 (2018) 232–239.
- [9] S. Korte, T. Jüstel, *Mater. Res. Bull.* 104 (2018) 27–37.
- [10] X.J. Kang, W. Lu, H.C. Wang, D.X. Ling, *Mater. Res. Bull.* 108 (2018) 46–50.
- [11] P. Dorenbos, *J. Lumin.* 91 (2000) 155–176.
- [12] P. Dorenbos, *Phys. Rev. B* 62 (2000) 15640.
- [13] P. Dorenbos, *Phys. Rev. B* 62 (2000) 15650.
- [14] P. Dorenbos, *Phys. Rev. B* 64 (2001) 125117.
- [15] P. Dorenbos, *J. Lumin.* 99 (2002) 283–299.
- [16] B. Dickens, L.W. Schroeder, W.E. Brown, *J. Solid State Chem.* 10 (1974) 232–248.
- [17] L. Jiang, R. Pang, D. Li, W. Sun, Y. Jia, H. Li, J. Fu, Ch Li, S. Zhang, *Dalton Trans.* 44 (2015) 17241–17250.

- [18] T. Nakajima, T. Tsuchiya, *ACS Appl. Mater. Interfaces* 7 (2015) 21398–21407.
- [19] C.H. Huang, T.M. Chen, *Opt. Express* 18 (2010) 5089–5099.
- [20] N. Guo, H. You, Y. Song, M. Yang, K. Liu, Y. Zheng, Y. Huang, H. Zhang, *J. Mater. Chem.* 20 (2010) 9061–9067.
- [21] C.H. Huang, T.M. Chen, W.R. Liu, Y.C. Chiu, Y.T. Yeh, S.M. Jang, *ACS Appl. Mater. Interfaces* 2 (2010) 259–264.
- [22] M. Trevisani, K.V. Ivanovskikh, F. Piccinelli, A. Speghini, M. Bettinelli, *J. Phys. Condens. Matter* 24 (2012) 385502.
- [23] D.E. Wagner, K.M. Eisenmann, A.L. Nestor-Kalinowski, S.B. Bhaduri, *Acta Biomater.* 9 (2013) 8422–8432.
- [24] S.J. Sun, Z.B. Lin, L.Z. Zhang, Y.S. Huang, G.F. Wang, *J. Alloys. Compd.* 551 (2013) 229–232.
- [25] O.L. Vorontsova, A.P. Malakho, V.A. Morozov, S.Y. Stefanovich, B.I. Lazoryak, *Russ. J. Inorg. Chem.* 49 (2004) 1793–1802.
- [26] E.S. Zhukovskaya, D.V. Deyneko, O.V. Baryshnikova, A.A. Belik, I.I. Leonidov, A.V. Ishchenko, S.Y. Stefanovich, V.A. Morozov, B.I. Lazoryak, *J. Alloys. Compd.* 787 (2019) 1301–1309.
- [27] O.V. Baryshnikova, A.P. Malakho, K.K. Kobyletskii, A.A. Fursina, O.N. Leonidova, V.A. Morozov, I.A. Leonidov, S. Yu Stefanovich, B.I. Lazoryak, *Russ. J. Inorg. Chem.* 50 (2005) 823–832.
- [28] A.V. Teterskii, S.Y. Stefanovich, B.I. Lazoryak, D.A. Rusakov, *Russ. J. Inorg. Chem.* 52 (2007) 308–314 and references therein.
- [29] A.A. Belik, V.A. Morozov, D.V. Deyneko, A.E. Savon, O.V. Baryshnikova, E.S. Zhukovskaya, N.G. Dorbakov, Y. Katsuya, M. Tanaka, S.Y. Stefanovich, J. Hadermann, B.I. Lazoryak, *J. Alloys. Compd.* 699 (2017) 928–937.
- [30] A. Benarafa, M. Kacimi, G. Coudurier, M. Ziyad, *Appl. Catal. A Gen.* 196 (2000) 25–35.
- [31] D.V. Deyneko, I.V. Nikiforov, B.I. Lazoryak, D.A. Spassky, I.I. Leonidov, S.Y. Stefanovich, D.A. Petrova, S.M. Aksenov, P.C. Burns, *J. Alloys. Compd.* 776 (2019) 897–903.
- [32] D.V. Deyneko, V.A. Morozov, J. Hadermann, A.E. Savon, D.A. Spassky, S.Y. Stefanovich, A.A. Belik, B.I. Lazoryak, *J. Alloys. Compd.* 647 (2015) 965–972.
- [33] G. Boulon, A. Collombet, A. Brenier, M.-T. Cohen-Adad, A. Yoshikawa, K. Lebbou, J.H. Lee, T. Fukuda, *Adv. Funct. Mater.* 11 (2001) 263–270.
- [34] X.L. Dong, J.H. Zhang, L.L. Zhang, X. Zhang, Z.D. Hao, Y.S. Luo, *Eur. J. Inorg. Chem.* 2014 (2014) 870–874.
- [35] J. Cui, L. Wang, Q.F. Shi, Y. Tian, P. Huang, C.E. Cui, *Polyhedron* 141 (2018) 284–288.
- [36] X.L. Dong, J.H. Zhang, X. Zhang, Z.D. Hao, Y.S. Luo, *J. Lumin.* 148 (2014) 60–63.
- [37] Q.X. Yu, L. Wang, P. Huang, Q.F. Shi, Y. Tian, C.E. Cui, *J. Mater. Sci. Mater. Electron.* (2019), <https://doi.org/10.1007/s10854-018-0501-3>.
- [38] B. Ma, K. Su, Q.X. Zhang, Y.P. Shi, B.W. Xiong, X.Q. Ma, *J. Lumin.* 204 (2018) 626–632.
- [39] R. Shi, X. Wang, Y. Huang, Y. Tao, L. Zheng, H. Liang, *J. Phys. Chem. C* 122 (2018) 7421–7431.
- [40] O. Sidletskiy, V. Kononets, K. Lebbou, S. Neicheva, O. Voloshina, V. Bondar, V. Baumer, K. Belikov, A. Gektin, B. Grinyov, M.F. Joubert, *Mater. Res. Bull.* 47 (2012) 3249–3252.
- [41] Y. Tao, Y. Huang, Z. Gao, H. Zhuang, A. Zhou, Y. Tan, D. Li, S. Sun, *J. Synchrotron Radiat.* 16 (2009) 857–863.
- [42] A.A. Belik, F. Izumi, T. Ikeda, M. Okui, A.P. Malakho, V.A. Morozov, B.I. Lazoryak, *J. Solid State Chem.* 168 (2002) 237–244.
- [43] A.A. Belik, F. Izumi, T. Ikeda, B.I. Lazoryak, V.A. Morozov, A.P. Malakho, S.Y. Stefanovich, V.V. Grebenev, O.V. Shelmenkova, T. Kamiyama, K. Oikawa, I.A. Leonidov, O.N. Leonidova, S.A. Davydov, *Phosphorus Sulfur Silicon Relat. Elem.* 177 (2002) 1899–1902.
- [44] R.D. Shannon, C.T. Prewitt, *Acta Crystallogr. Sect. B* 25 (1969) 925–946.
- [45] Y.Q. Jia, *J. Solid State Chem.* 95 (1991) 184–187.
- [46] A.A. Belik, M. Azuma, M. Takano, *Solid State Ion.* 172 (2004) 533–537.
- [47] B.Y. Huang, B.L. Feng, L. Luo, C.L. Han, Y.T. He, Z.R. Qiu, *Mater. Sci. Eng. B-Adv. Funct. Solid-State Mater.* 212 (2016) 71–77.
- [48] B. Henderson, G.F. Imbush, *Optical Spectroscopy of Inorganic Solids*, Clarendon Press, Oxford, 1989.
- [49] A.E. Hughes, *J. Phys.-Colloq.* 28 (1967) C4-55–C4-65.
- [50] L. Schwarz, B. Finke, M. Kloss, A. Rohmann, U. Sasum, D. Haberland, *J. Lumin.* 72–74 (1997) 257–259.
- [51] T. Shalapska, G. Stryganyuk, A. Gektin, P. Demchenko, A. Voloshinovskii, P. Dorenbos, *J. Phys. Condens. Matter* 22 (2010) 485503.
- [52] K. Ivanovskikh, A. Meijerink, C. Ronda, F. Piccinelli, A. Speghini, M. Bettinelli, *Opt. Mater.* 34 (2011) 419–423.